J. Geomag. Geoelectr., **47**, 213–229, 1995

A New-Type Source of Power Line Harmonic Radiation Possibly Located on the Kola Peninsula

Ichiro TOMIZAWA, Hayato NISHIDA*, and Takeo YOSHINO

Department of Electronic Engineering, The University of Electro-Communications, 1-5-1 Chofugaoka, Chofu-shi, Tokyo 182, Japan

(Received January 14, 1994; Revised November 7, 1994; Accepted November 7, 1994)

A new-type source of power line harmonic radiation (PLHR) is described in this paper to point out its significance to the magnetospheric emissions. Characteristic electromagnetic fields were observed over the Kola Peninsula, northern Russia, during the flight of the balloon B_{15}-2N in 1982. The source is characterized by (a) the fundamental frequency of 24.4 Hz, (b) the harmonic spectrum continuously extending up to VLF, and (c) the isolation from commercial power lines. These characteristics are different from the previously reported PLHR sources that could trigger the magnetospheric emissions. Based on the low impedance field and the amplitude variation along the balloon trajectory, the source can be modeled by a horizontal electric dipole or a horizontal magnetic dipole, and then the source distance is estimated within the induction area of a few hundred kilometers. The most probable source is an electric railroad or a single-phase power line, driven by an isolated power generator, and located on the Kola Peninsula. Estimating the radiation power through the ionosphere, it is shown that enough power to trigger magnetospheric emissions may be radiated into the magnetosphere from the source. Therefore, it is suggested that the source can be recognized as a new-type PLHR source possibly related to magnetospheric emissions.

1. Introduction

Power line harmonic radiation (PLHR) at the ELF/VLF band sometimes triggers magnetospheric emissions (Helliwell *et al.*, 1975; Luette *et al.*, 1977; Park and Helliwell, 1978; Bullough, 1983; Yoshino *et al.*, 1989; Parrot, 1990). Therefore, the PLHR field at the ELF/VLF band has been considered as an important source in the wave-particle interaction process in the magnetospheric emissions. Even at the fundamental frequency of commercial power lines, enhancements of electric field strength were explained as the excitation of the ionosphere by induction fields of power lines (Parrot *et al.*, 1991; Molchanov *et al.*, 1991). Therefore, the PLHR fields play an important role both in the ionosphere and in the magnetosphere.

However, actual PLHR electromagnetic fields below the ionosphere have not been investigated in details since it is difficult to estimate the characteristics of radiation from power lines on the ground due to local interferences of power lines. To overcome the local interferences, we have investigated the induced and radiated fields of power line systems by using balloons, rockets, and a satellite (Tomizawa and Yoshino, 1980, 1984; Yoshino and Tomizawa, 1981; Tomizawa *et al.*, 1985) in order to make a source model and to reveal the effects of PLHR on the electromagnetic environment. For the study of the PLHR field in the Scandinavian countries in connection with the geomagnetic activities, we conducted balloon observations of ELF electromagnetic fields (Tomizawa and Yoshino, 1984; Tomizawa *et al.*, 1985). The balloons were provided by the National Institute of Polar Research (NIPR), Japan to observe ELF and VLF electromagnetic fields, auroral X-ray radiations, and electrostatic fields (Fukunishi and Miyaoka, 1984). We found strong enhancements of power-line-induced electromagnetic fields at 300, 450 and 600 Hz

*Current address: NHK Science and Technical Research Laboratories, 1-10-11, Kinuta, Setagaya-ku, Tokyo 157, Japan.

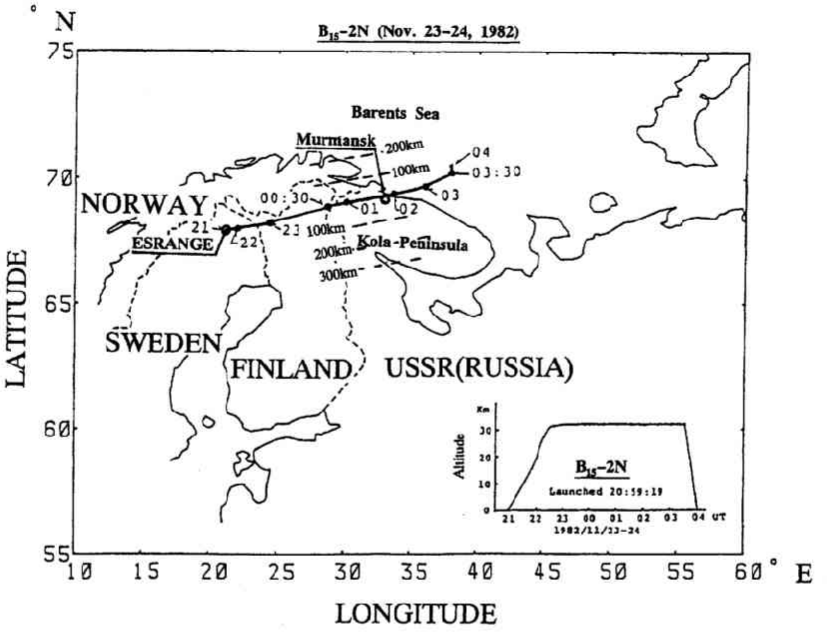

Fig. 1. The trajectory and the altitude level of the balloon B_{15}-2N. The balloon was launched from ESRANGE, Sweden, on November 23, 1982, and flew over the northern Scandinavia and the Kola Peninsula, and to the Barents Sea. The altitude during the flight is indicated in the lower right corner.

during the geomagnetic disturbance (Tomizawa *et al.*, 1985).

In this experiment, peculiar harmonic spectra in the magnetic field were observed by the balloon B_{15}-2N when it flew over the Kola Peninsula (Fig. 1), because the fundamental frequency is 24.4 Hz. In the previous analysis, we ignored these harmonic fields as a kind of internal interference, since the spectral characteristics of a DC-DC converter, a chopper amplifier, or a clock generator were quite similar to these observed ones. However, the observed harmonic field seemed uncorrelated with a kind of interferences, not only because the harmonics of 24.4 Hz appeared only in the magnetic field spectra, but also because the strength was not constant in time. Critically examining the possibility of interferences from the onboard instrument, we have concluded that the 24.4 Hz signal observed on the balloon was not caused by such interferences but by the induced harmonics of the signals (Tomizawa *et al.*, 1987). If the fundamental frequency is exactly at half the power line frequency of 50 Hz, the observed fields can be directly related to a commercial power line system as sub-harmonics. However, we could clearly show the difference between the generation frequency of 24.4 Hz and half the frequency of the commercial power line system generated exactly at 50 Hz. Thus, we have started to investigate characteristics of the harmonic fields and a location of the source.

In this paper, at first, the observed characteristics of 24.4 Hz, its harmonic fields, and the waveforms are presented, secondly, results of the model calculation for four elementary dipole sources are discussed to explain the observed characteristics of amplitude variation and wave impedance, and conclusively, the observed new-type PLHR source is suggested as a possible source of the PLHR emission in the magnetosphere.

2. Observed Results

2.1 Spectral characteristics

Figure 2 shows an example of the spectrum below 200 Hz observed on the balloon B_{15}-2N on No-

vember 24, 1982. Spectral lines at 24.4 Hz and its harmonic frequencies can be clearly recognized in the magnetic field spectrum of Fig. 2(a). However, corresponding spectral lines cannot be detected in the electric field spectrum of Fig. 2(b). The magnetic field strength of each harmonic field is indicated by dB relative to 1 A/m. (The value of 1 A/m can be converted to the flux unit as 1.26×10^{-6} T.) The electric field strength is indicated by dB relative to 1 V/m. Spectral lines of 50 Hz and its harmonic frequencies, caused by the commercial power line system, are detected both in the magnetic and the electric fields. It is important to note that the observed harmonic spectra indicate the narrow spectral lines. Therefore, the source of harmonic spectra is considered as stable as producing such a narrow spectral line. According to the results of inspection on the harmonic structures (Tomizawa *et al.*, 1987), the observed spectral harmonic structures are definitely related to the generation source apart from the balloon, that is, to the source placed on the earth. Therefore, source characteristics can be revealed by the analyses of the observed electromagnetic fields.

The harmonic spectra of the magnetic field up to 1 kHz are shown in Fig. 3 for the successive seven data intervals indicated below. The length of each data interval is 50 seconds. It is clearly seen that the harmonic spectral lines are continuously appearing as the horizontal narrow-spacing dark streaks and that

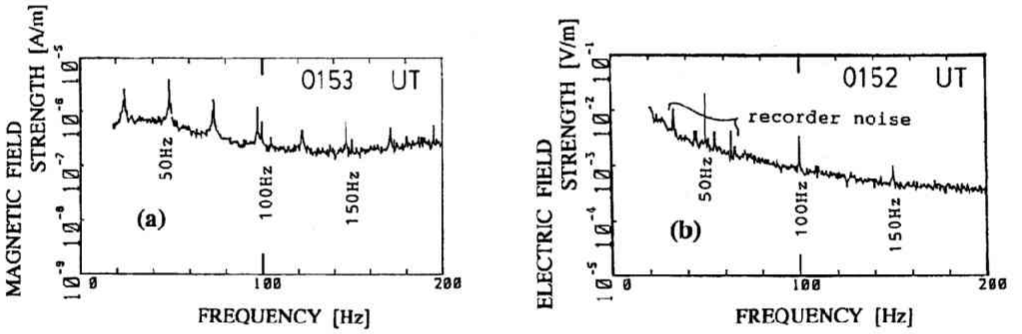

Fig. 2. (a) The magnetic field spectrum at 01h53m UT on November 24, 1982. The fundamental and harmonic line spectra of 24.4 Hz are clearly seen together with those of 50 Hz that are caused by the commercial power line system. Note that, below 50 Hz, the field strength are decreased by the characteristic of HPF. (b) The electric field spectrum at 01h52m UT. No line spectrum corresponding to 24.4 Hz is seen in this spectrum. However, line spectra relating to the commercial power line system are clearly seen at 50, 100 and 150 Hz. Note that the recorder noise appears below 70 Hz.

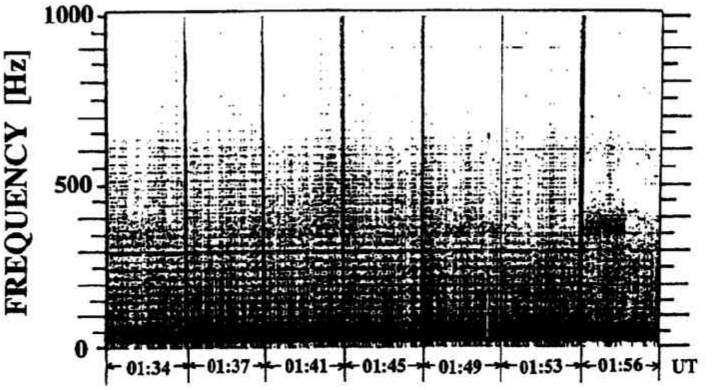

Fig. 3. Dynamic spectra of the magnetic field up to 1 kHz for the successive seven data intervals. Horizontal narrow-spacing streaks are indicating the harmonic spectral lines of 24.4 Hz.

the harmonic spectra sometimes extend up to 1 kHz that is the upper limit of this observation. Therefore, it is normal to consider that the harmonic spectra extend to much higher frequencies.

To investigate the time variation of these harmonic spectra, the spectra of the magnetic and electric fields are shown in time series from 01h00m to 02h30m UT in Fig. 4. The harmonic frequencies of 24.4 Hz are clearly seen almost all of these magnetic field spectra in Fig. 4(a), while the harmonic field cannot be seen in the electric field component in Fig. 4(b). Note that the dotted vertical lines in these figures are indicating the harmonic frequencies of the commercial power line system, that is 50, 100, and 150 Hz, in Murmansk city, USSR (currently Russia). As seen from the trajectory of the balloon shown in Fig. 1, the increase in the harmonic fields of 50 Hz around 2h UT was caused by the power line system of Murmansk

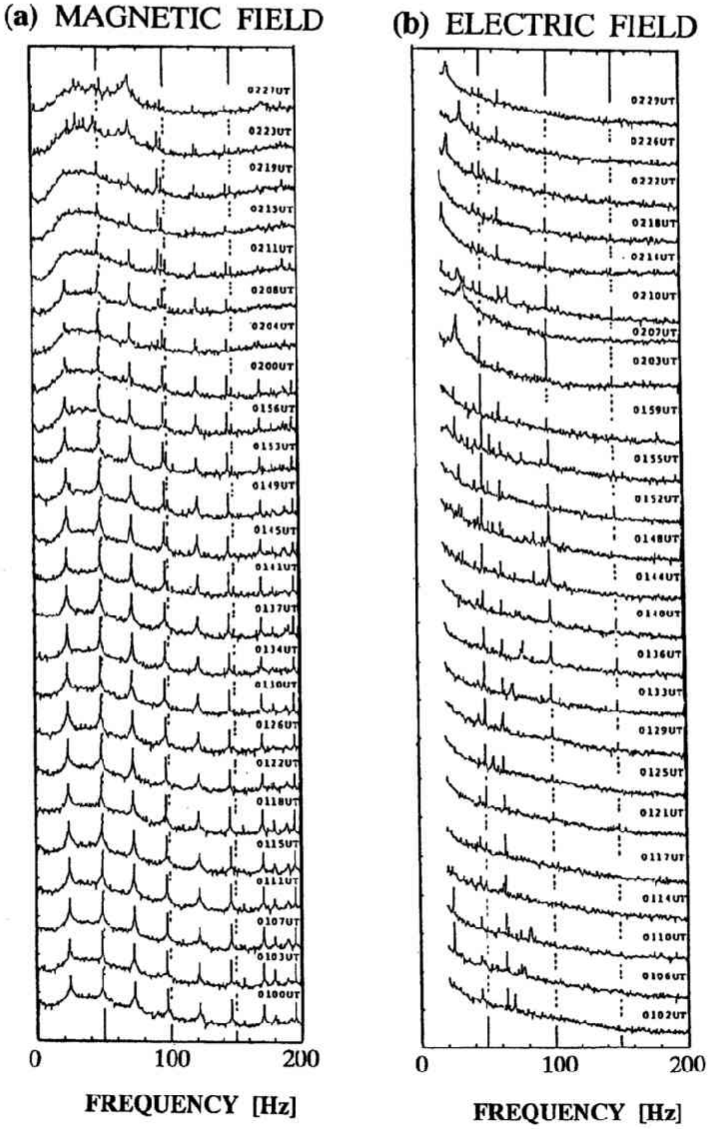

Fig. 4. (a) Dynamic spectra of the magnetic field component from 01h00m to 02h27m UT. (b) Dynamic spectra of the electric field component. Note that the vertical broken lines indicate the harmonic frequencies of the commercial power line system, i.e. 50, 100 and 150 Hz.

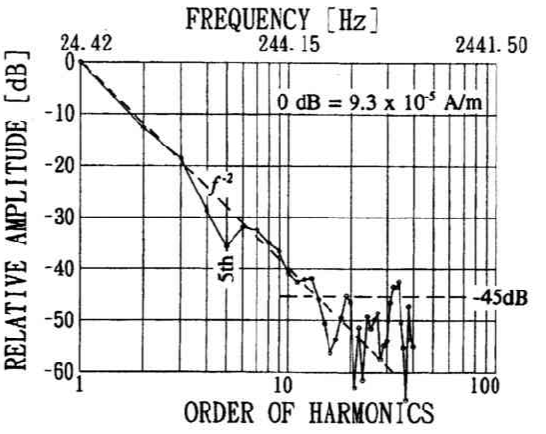

Fig. 5. Relative magnetic field strength of harmonics up to 40th (~1 kHz) compared to the fundamental field strength. The field strength is already compensated for the frequency characteristics of HPF of f_c = 40 Hz.

city. However, the harmonic fields of 24.4 Hz show their peaks around 01h30m UT when the balloon was flying over the western suburb of Murmansk city, as seen in Fig. 1. Thus, the cause of the harmonic fields of 24.4 Hz may be independent of the commercial power line system in Murmansk city.

Note that the lower part of the magnetic spectra, less than 50 Hz, was attenuated in amplitude by the 40 Hz HPF placed at the top of the receiver (Tomizawa *et al.*, 1987). After compensating the frequency characteristics both of the receiver and of the telemetry system, the relative field strengths of the harmonic frequencies are shown in Fig. 5 for the period of 01h22m43s to 01h23m40s UT. The open circle indicates the relative field strength of each harmonic field strength with respect to the field strength of the fundamental frequency of 9.3×10^{-5} A/m. The field strength of the harmonic frequencies steeply decreases with increasing the order of harmonic number by f^{-2} up to the 10th order, while the amplitudes for harmonic frequencies of more than 10th order seem rather constant at approximately –45 dB. It seems reasonable to expect that harmonic fields of more than 1 kHz exist at approximately –45 dB since the observed higher harmonics indicate a rather flat spectral characteristic. The small dip at the 5th order can be interpreted as a waveform distortion as long as one fifth of a single cycle of sinusoidal waveform because the Fourier analysis of such distortion will make a ripple every five order in amplitude spectrum. Therefore, the waveform can be basically expressed by a distorted sinusoidal wave, because the amplitude of the fundamental frequency is the strongest component of all harmonics and because the harmonic amplitude steeply decreases at lower harmonics in spectrum. The actual distorted sinusoidal waveform will be illustrated in Fig. 8 and described in Subsection 2.3.

2.2 Amplitude variation of each harmonic field along the balloon trajectory

Extracting the harmonic components of 24.4 Hz from Fig. 4, the time variations of each harmonic field of 24.4 Hz during the flight of the balloon, from 23rd to 24th of November, 1982, are obtained as Fig. 6. The order of the harmonic field is indicated by the attached number of each curve. All of these harmonic fields show gradual increases from 23h30m to 01h00m UT, broad peaks around 01h30m UT, and relatively steep decreases after 01h30m UT. It is important that the observed amplitude of the harmonics shows an asymmetrical shape of variation along the trajectory. As the trajectory of the balloon on the map indicates a straight line through the flight, it can be interpreted that the observation is made in a one-dimensional survey. Judging from the background noise level at 24.4 Hz indicated by the horizontal broken line, the actual field strength can only be seen from 23h40m to 02h10m UT when the balloon had been flying over the Kola Peninsula, as shown in Fig. 1. The maximum Signal-to-Noise ratio (S/N) at 24.4 Hz is 12 dB at 01h30m UT.

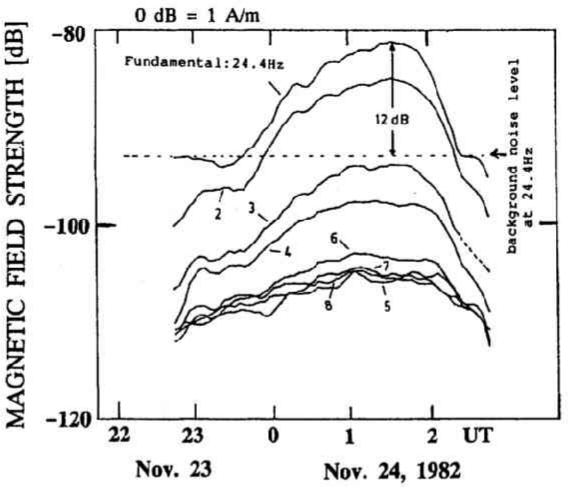

Fig. 6. Time variation of the fundamental and harmonic field strengths. The field strength is shown in dB with respect to 1 A/m. The numbers attached to each curve indicate the order of harmonics. Horizontal broken line indicate the background noise level at 24.4 Hz.

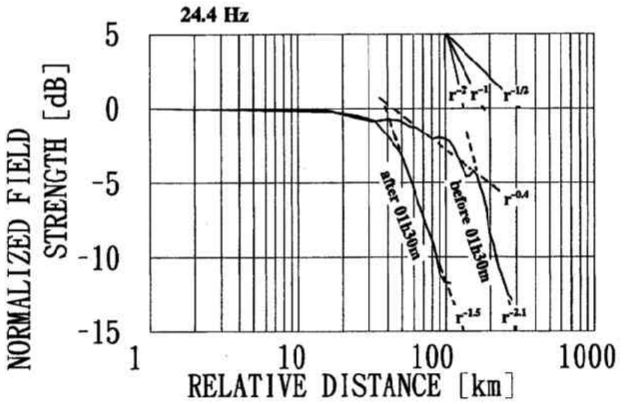

Fig. 7. Relative amplitude variation with respect to the maximum point at 01:30 UT. The distance are measured from the maximum point.

To investigate the source location, radial amplitude variation rates should be examined first. However, it is impossible to obtain the radial distance since the actual source location is unknown. Then, we assume at first that the transmission source were located at or close to the place of the maximum. Figure 7 shows amplitude variation of 24.4 Hz with respect to the location of 01h30m UT. The amplitude is normalized to the value at 01h30m UT. It is clearly seen that the amplitude variation is asymmetrical with respect to the maximum since the curve indicated as "before 01h30m" is largely separated from that indicated as "after 01h30m", and since the decreasing rate for two curves are quite different. For example, the maximum decreasing rate for "before 01h30m" is $r^{-2.1}$, but that for "after 01h30m" is $r^{-1.5}$, where r is the radial distance from the source. These decreasing rates are much higher than $r^{-1/2}$ of the propagation mode (Ginzberg, 1974), which means the observation was made in the near field region. If the source can be a simple dipole of point source, a directivity for an opposite direction is the same since the amplitude depends on a sine or cosine function (Galejs, 1972). As the amplitude variation is quite different for the

opposite direction as shown in Fig. 7, the difference cannot be explained by a directivity of any dipole. Therefore, it is interpreted that the source should be located apart from the balloon trajectory. The range of distance will be discussed later in Subsection 4.3.

2.3 Wave impedance

From Fig. 2, the observed magnetic field strength and the upper limit of the electric field strength can be obtained. The electric field strength at 24.4 Hz is less than 5×10^{-3} V/m, and the magnetic field strength at 24.4 Hz is 4×10^{-6} A/m. After compensating the frequency characteristic of the observation system of 17 dB at 24.4 Hz, the magnetic field strength becomes 2.8×10^{-5} A/m. Therefore, the wave impedance, calculated from the ratio between the electric field strength and the magnetic field strength, should be less than 180 Ω. On the other hand, the wave impedance of the power line induction field at 50 Hz are 2000 Ω that is calculated by using the field strengths in Fig. 2. Note that the noise level of the electric field component does not indicate the actual background noise level at the ELF band since the dynamic range of the total receiver system for the electric field component was limited by the low S/N of the FM-FM telemetry channel (Tomizawa *et al.*, 1987). Then, the actual background electric field strength should be less than the indicated strength in Fig. 2. To improve S/N, we have introduced a coherent integration of the waveform since the spectral line is enough narrow to be considered as a coherent wave, and have coherently integrated by folding in the time sequence of the fundamental period during the 30-second interval. By adjusting the fundamental period to increase the amplitude of the resulting waveform, the best fitted fundamental frequency is obtained as 24.415 Hz. Figure 8(a) shows one cycle of the integrated waveform of the magnetic field obtained by using the above procedure. The shape of the waveform is quite different from a sinusoidal waveform, especially the latter half of the cycle indicates an impulsive peak. The integration procedure is also applied to the electric field component in the same period, as shown in Fig. 8(b). The integration during the 30-second interval gives the improvement of S/N by 15.6 dB

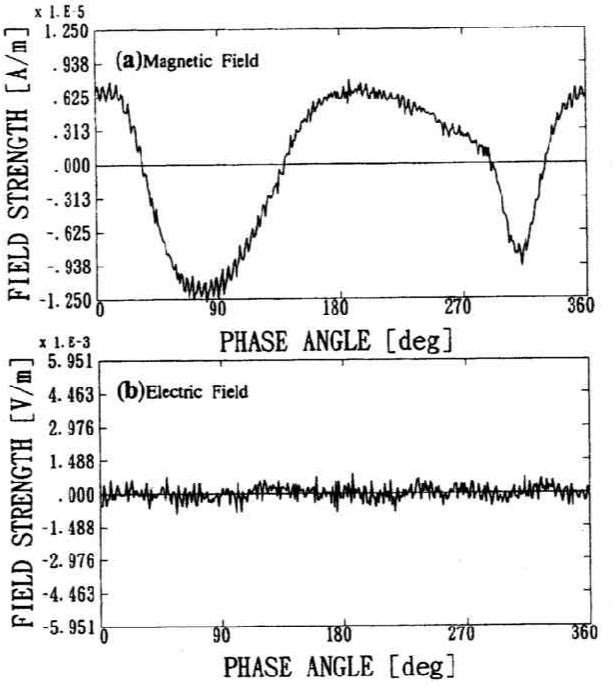

Fig. 8. (a) Waveform of the 24.4 Hz magnetic field after the folding integration through the 30-sec data. (b) Corresponding electric field waveform. However, electric field waveform does not show correlating variation.

compared with the FFT analysis. In spite of the improvement in S/N for the electric field component, it is impossible to identify a corresponding shape of waveform. The field strength of the electric field component at 24.415 Hz is estimated as 15.6 dB less than the first estimated threshold value of 5×10^{-3} V/m according to the spectrum of Fig. 2(b). Therefore, the second estimation of the upper limit of the electric field strength is 8.3×10^{-4} V/m. As the magnetic field strength at 01h53m is already determined as 2.8×10^{-5} A/m from Fig. 2, the wave impedance is estimated as less than 30 Ω. If the upper limit value of the electric field is constant, the wave impedance value becomes as low as 9 Ω when the magnetic field strength shows the maximum value of 9.3×10^{-5} A/m at 01h30m UT. The upper limit of the wave impedance of 30 Ω can be applied through the period from 23h40m to 02h10m UT. Therefore, the observed field is considered as a low source impedance field because the wave impedance is lower than 377 Ω in the free space.

3. Model Calculation for Four Elementary Dipoles

3.1 Calculation model

The propagation at ELF waves has been formulated by Galejs (1972) for four types of elementary dipoles in the geometrical configuration shown in Fig. 9. We have assumed the source of the 24.4 Hz field as a point source in order to reduce the observed characteristics to a simple problem. Four elementary dipole sources, i.e. a vertical electric dipole (VED), a vertical magnetic dipole (VMD), a horizontal electric dipole (HED), and a horizontal magnetic dipole (HMD), are considered as a possible point source. Electromagnetic fields at the ELF band propagate in the thin spherical shell that is terminated by the ground surface and the bottom of the ionosphere. At the ELF band the curvature of the earth should be taken into the formulation since the wavelength is comparable to or lager than the earth radius. A dipole source is placed at $S\ (a + Z_s, 0, 0)$, where a is the earth radius and Z_s is a height of the source above the ground surface. A receiver is placed at $P\ (a + Z, \theta, \phi)$, where Z is a receiver altitude. The height of the

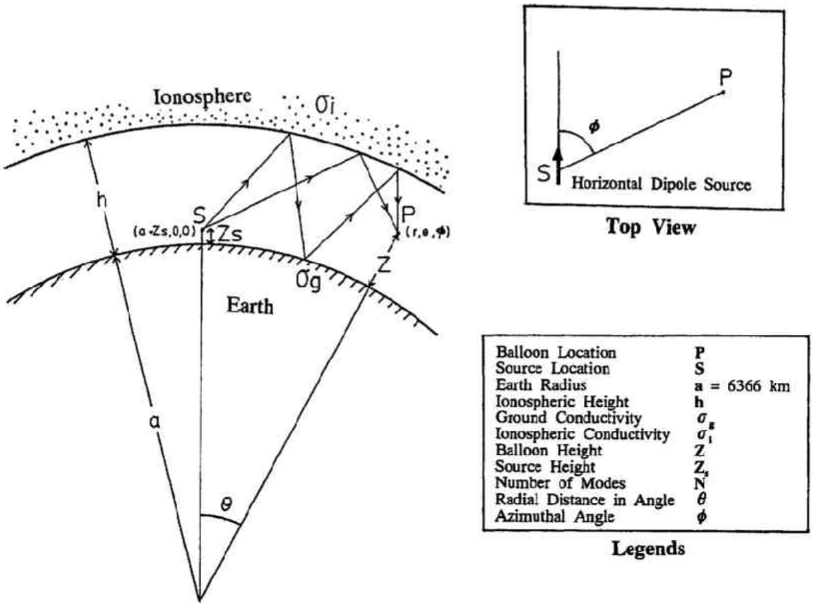

Fig. 9. Geometry for the calculation of the electromagnetic fields produced by the 24.4 Hz source at the location *S*. For a horizontal dipole, the azimuthal angle from the dipole axis ϕ is measured in the eastward rotation angle from the dipole axis as shown in the box of Top View.

ionosphere is h, which is approximately 60 km at 25 Hz in the daytime and is approximately 80 km in the nighttime (Galejs, 1972; Katan and Bannister, 1987). However, the height of the nighttime ionosphere can be changed by the auroral activity in the auroral zone since precipitating high energy particles excite secondary electrons and ions at lower altitude than the E layer and expand the ionosphere downward (Katan and Bannister, 1987). Although the geomagnetic activity was relatively high just before 23h UT on November 23, 1982, it had been relatively quiet after 23h UT (Fukunishi and Miyaoka, 1984). Thus the ionospheric height during the balloon flight after 23h UT is assumed to be stably placed at 80 km. The ionospheric conductivity σ_i is assumed as 10^{-5} S/m, and the ground conductivity σ_g is assumed as 10^{-3} S/m through this analysis.

Calculations of electromagnetic fields and wave impedances that are defined as the ratios of the vertical electric field to the horizontal magnetic field are made according to the calculation formulas for the ELF propagation described in Chapter 4 of Galejs (1972). Characteristics of this calculation are somewhat different from Galejs (1972) since the receiver altitude is at 30 km above the ground surface. Most of the calculations at the ELF band has been made at or under the ground surface (Wait, 1970; Bannister, 1986).

3.2 Radial variations of horizontal magnetic field strength

Figure 10 shows radial variations of horizontal magnetic field strength for four elementary dipoles using the calculation parameters presented at the top. Note that the magnetic field strength is normalized to a dipole moment of unit value. As described by Ginzberg (1974), the horizontal magnetic field decreases at $r^{-1/2}$, where r is the radial distance from the transmitter, at the distance more than 1000 km for 56 Hz. The decreasing rate is used as the indicator of the radiation field. For VED in Fig. 10(a), the field can be considered as radiation field even at 100 km, since the decreasing rate becomes $r^{-1/2}$. For VMD in Fig. 10(b), the minimum distance of radiation field is 200 km. However, for HED in Fig. 10(a) and HMD in Fig. 10(b), the decreasing rate gradually approaches to $r^{-1/2}$ even at 1000 km, except for the case of 0 deg for HED and 90 deg for HMD. Therefore, the horizontal magnetic field for HED and HMD within 1000

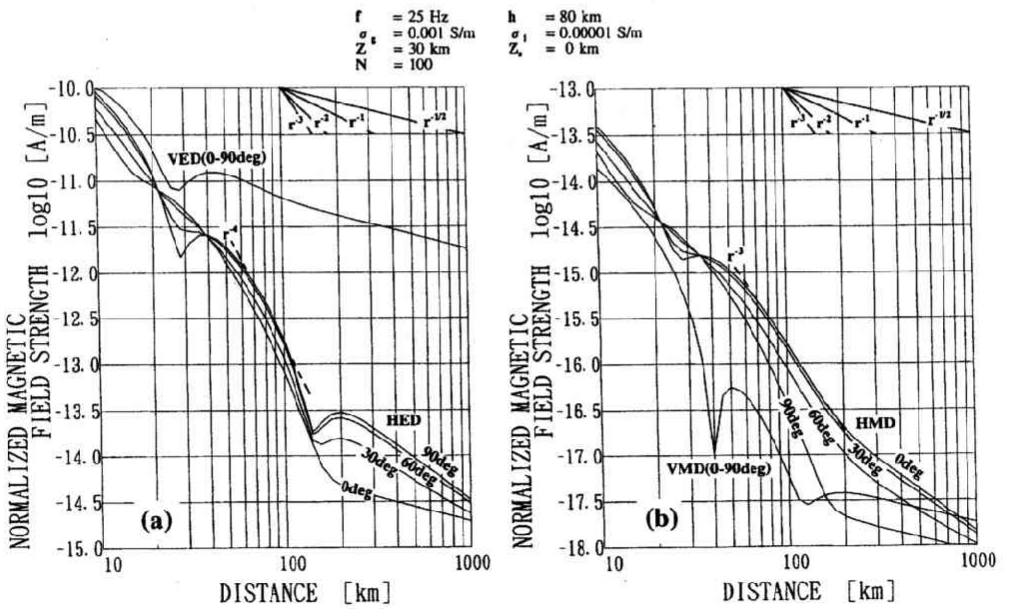

Fig. 10. Calculated horizontal magnetic field strength with respect to radial distance (a) for VED and HED, and (b) for VMD and HMD, at the balloon height. The magnetic field strength is normalized to a dipole moment.

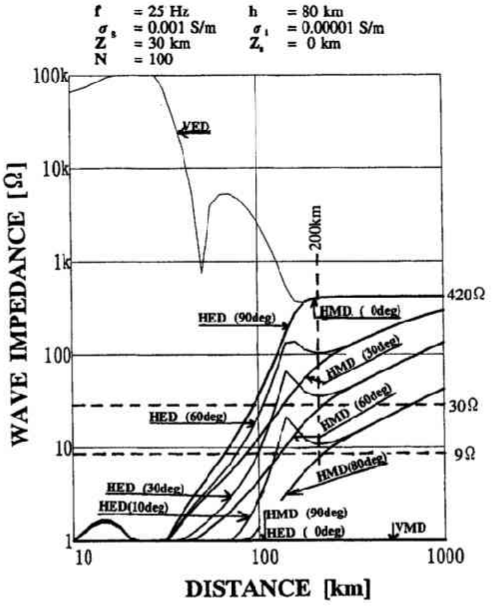

Fig. 11. Wave impedance versus distance from the four elementary types of dipole sources. The calculation parameters are shown at the top of this figure. Azimuthal angles for the horizontal dipoles are indicated in parentheses. The upper limit of the observed wave impedance of 30 Ω for the period from 0h to 2h UT is indicated in the horizontal dashed line. Additionally the minimum upper-limit value of wave impedance of 9 Ω at 01h30m UT is also indicated.

km is interpreted as a induction region.

It is important to note that decreasing rates for HED, VMD and HMD within 200 km are high compared with the radiation region, and quite variable for direction angles for HED and HMD.

3.3 Radial variations of wave impedance

In Fig. 11, wave impedance vs. radial distance from the possible four types of dipoles is different especially in the near field region. The wave impedance for HED and HMD depends on the direction angle of ϕ that is measured in clockwise from north, as illustrated in Fig. 9. To show the dependence on the angle ϕ, the wave impedance curves at 0, 30, 60, 80 and 90 degrees for HMD, and at 0, 10, 30, 60 and 90 degrees for HED, are presented with the parentheses attached to the dipole names, e.g. HED(30deg), as shown in Fig. 11. It is interesting to note that the overall shape of the wave impedance for these two horizontal dipole sources are quite similar if each direction angle is subtracted from 90°. In other words, the overall shape of the wave impedance for the two horizontal dipoles is interpreted as a kind of complementary dipole if a sine factor is exchanged with a cosine factor. However, a definitive difference is seen in the short interval between 100 and 200 km. The wave impedance for HED is higher than that for HMD except 90° or 0°. It can be explained by the difference of the excitation modes of each dipole source. As these higher modes are attenuated in the distance greater than 200 km, the impedances of two dipoles show a good agreement.

4. Discussion

4.1 Source mechanism estimated by the spectral characteristics

The observed spectral characteristics is discussed here in relating to a physical source. As shown in Subsection 2.1, the observed harmonic spectra and the estimated waveform indicate a highly distorted waveform at the source. Three possible mechanisms are generally studied as generating such harmonic fields; 1) an electric power transmission line, 2) an electric railroad, 3) an artificial transmitter. These

possible mechanisms can be further divided into more detailed mechanisms because they can be operated in either AC or DC system. However, the difference of DC and AC is only containing the DC component or not. Therefore, we do not divide the source mechanism by DC or AC. On the other hand, the AC power transmission line can be further divided into two kinds of system; a single-phase or three-phase system. However, the continuous harmonic spectrum cannot be obtained by the three-phase type power transmission system because the multiplication of three, i.e. 3, 6, 9, and so on, are especially enhanced around the three-phase transmission lines (Tomizawa and Yoshino, 1984; Tomizawa *et al.*, 1985). A single phase transmission line can produce such a harmonic structure as well as a AC railroad if there were a highly distorted current. If there is an unknown artificial transmitter like the SANGUINE project (Katan and Bannister, 1987), the spectrum can easily be generated. However, the possibility of an unknown transmitter may not be expected since such a highly distorted waveform of the transmission system would not result in an efficient communication. Thus, we can expect two possible candidates for the generation mechanisms; a) a single-phase power transmission line, b) an electric railroad.

On the other hand, it is important to note that the frequency of 25 Hz has been used in the electric railroad in some countries (Denki-gakkai-tsuushin-kyou-iku-kai, 1971). But it is not known now whether such a railroad exists in Russia. As the frequency difference between 24.4 Hz and 25 Hz is only 0.6 Hz (2.4% of 25 Hz), it can be considered that the two frequencies are consistent. If the frequency of 24.4 Hz is generated by an isolated power generator that is not synchronized to the commercial power lines at Murmansk city, the frequency difference can be explained easily.

The observed characteristic frequency can easily be related to an electric railroad, since it is one of the possible candidates described above. However, an excitation by a single-phase power line is still possible because we cannot find out a causal railroad in the literature till now. Further studies are requested to search for a causal source like a railroad or a power line along the balloon trajectory.

4.2 Possible source models estimated by the wave impedance and the amplitude variation

Possible source models will be discussed here based (1) on the amplitude variation and (2) on the wave impedance.

(1) *Amplitude variation*: As the balloon flew in the same direction in the constant speed of 130 km/h through this flight, as seen in Fig. 1, the amplitude variation can be attributed to the characteristics of the source of 24.4 Hz if the source were stationary during this flight. If the induction field has an omnidirectional characteristic in two dimension, the one-dimensional observation of this field will give a symmetrical shape. Therefore, the observed asymmetrical shape of the field variation can be attributed to the directivity of the two-dimensional characteristic of the induction field. VED and VMD intrinsically indicate omnidirectional characteristics around the dipole sources, as shown in Fig. 10. Therefore, we could not expect any asymmetrical shape of the amplitude variation for a one-dimensional trajectory even passing far from the dipole. It is concluded that HED and HMD are a possible source of the observed asymmetrical amplitude variation since the two dipoles show a typical directivity like a shape of figure 8. Hence, the observed amplitude variation can be interpreted as a cross-section of the two-dimensional distribution.

(2) *Wave impedance*: Characteristics of wave impedances shown in Fig. 11 can be divided into two main regions at approximately 200 km. The wave impedance of VED is quite different from other three dipoles within 200 km from the source. It is more than several hundreds Ω while it is less than 420 Ω for other dipoles. Therefore, the electromagnetic field of VED within 200 km is called as a high impedance field, and those of VMD, HED, and HMD are called as low impedance fields. The wave impedance at the far region that is more than 200 km is relatively flat compared with the near region. The boundary of variations in the wave impedance approximately at 200 km is clearly seen on VED, HED(90deg) and HMD(0deg) because these three types of dipoles only excite TM-mode waves and higher components of the TM mode are attenuated within 200 km. The wave impedance for these dipoles in the far region is calculated as 420 Ω in this calculation, which is interpreted as the wave impedance for the propagation mode TM_0 at 24.4 Hz. The calculated wave impedance for the propagation mode at the ELF band is

determined by the wave propagation constant S (Galejs, 1972). The wave impedance η is determined as $\eta = S \cdot Z_0$, where Z_0 (= 377 Ω) is the wave impedance in vacuum. The propagation constant S is 1.12 that is almost equal to that of the propagation mode TM_0 at the ELF band (Galejs, 1972). Therefore, the impedance of 420 Ω is used as the reference value of the propagation mode.

The termination of the differences at the distance of 200 km is not so clearly seen for HED(60deg), HED(30deg), HED(10deg), HMD(30deg), HMD(60deg) and HMD(80deg) in Fig. 11. These curves gradually increase and approach to the wave impedance of the propagation mode, i.e. 420 Ω, by increasing distances because the ratio of the excited propagation mode of TM_0 to other attenuating modes is relatively small, compared with the case of HED(90deg) and HMD(0deg). However, sharp increases for HED(60deg), HED(30deg) and HED(10deg) are clearly terminated at approximately 200 km. The distance of 200 km is also considered as the boundary of two regions, and the wave impedances for the two dipoles with the angle of 30 or 60 degrees can be considered as an intermediate value. The wave impedances for VMD, HED(0deg) and HMD(90deg) shown in Fig. 11 are always less than 1 Ω from 10 to 1000 km, because no excitation of the propagation mode TM_0 is expected (Galejs, 1972). Therefore, the three-dipole source models, VMD, HMD and HED, are intrinsically characterized by the low impedance field.

Combining the results of discussion in (1) and (2), the two source models, HMD and HED, should be considered in the further studies.

4.3 Source distance estimated by the amplitude variation and the wave impedance

As described in Subsection 2.2, the amplitude variation cannot be explained by a dipole source located at or close to the maximum (01h30m UT), since the asymmetrical and different decrease is not expected for a trajectory passing just over a dipole source. Additionally, it is shown in Subsection 2.3 that the upper limit of the wave impedance is less than 30 Ω for the period from 23h40m to 02h10m UT. The observation range along the balloon trajectory is 320 km since the balloon flight speed is 130 km/h. Therefore, the angle of the receiver direction along the observation range must be kept within the limit of estimation. Based on the discussion in Subsection 4.2, the low impedance electromagnetic field is attributed to the induction field generated around dipole sources such as HMD and HED. The estimated source distance should be within the induction area of a few hundreds of km. However, as shown in Subsection 3.2, the wave impedances for HMD and HED vary depending on the direction angle ϕ. As the upper limit of the wave impedance is 30 Ω, the estimated upper limit of the distance between the source and the receiver can be determined by the crossing point with the horizontal dashed line indicated as 30 Ω in Fig. 11. For example, the estimated upper limit of the distance for HMD(60deg) is 210 km, and that for HED(30deg) is 120 km.

Then, a possible trajectory should be determined to satisfy the following conditions:

1) The whole trajectory of 320 km must be within the low-impedance region bounded by 30 Ω, which can be deduced from Fig. 11.

2) Amplitude difference between the maximum and the edge of the trajectory must be 12 dB, which is obtained from Fig. 6.

Figure 12 shows the low-impedance regions for HED and HMD that are deduced from Fig. 11. The low-impedance region looks like a corridor, but its width is narrower than the full length of the balloon trajectory of 320 km. It is, however, possible to obtain a various kind of trajectories within the low-impedance region if it is tilted. Although a trajectory can be placed anywhere within the region, the trajectory must satisfy the required condition (2) through the path. If a radial distance to the trajectory becomes closer, amplitude difference between the maximum at the foot point of the trajectory and the minimum at the far end of the trajectory. The difference can roughly be estimated from Fig. 10, provided that the longer leg of the trajectory in Fig. 12 is 200 km. The estimated amplitude differences against the radial distance to the foot point are presented in Table 1 for HED and HMD. The condition of 12 dB should be satisfied at approximately 100 km for HED, and at approximately 150 km for HMD. Therefore, it is concluded that the distance to the balloon trajectory should be approximately 100 to 150 km from a possible source. The possible range of distance, 100 to 150 km from the trajectory, is placed in the region

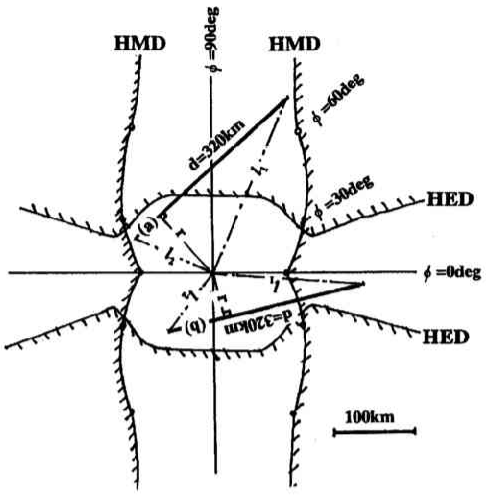

Fig. 12. Low wave-impedance regions bounded by 30 Ω for HED and HMD. An example of possible trajectory in each region is indicated by a bold short straight line.

Table 1. Estimated amplitude difference between the foot point and the far end for HED and HMD. Provided that the distance of the longer leg of the trajectory is 200 km.

r [km]	l_1 [km]	(HED) [dB]	(HMD) [dB]
10	200	70	70
20	201	60	50
50	206	40	35
100	223	10 to 20	20 to 30
150	250	−5 to 10	10 to 15
200	283	3 to 5	3 to 6
300	360	1 to 2	1 to 3

of the Kola Peninsula, as shown in Fig. 1. Hence, it is concluded that the new-type PLHR source is located on the Kola Peninsula.

4.4 Estimated radiation power into the magnetosphere

As described in Subsection 2.1, the higher order of harmonics more than 1 kHz would be existing and their spectral amplitudes are comparable at higher harmonic frequencies. Therefore, it is possible to predict that higher electromagnetic fields exist at higher harmonic frequencies because the efficiency of radiation at ELF to VLF bands increases with frequencies (Galejs, 1972). The wave length in vacuum at 3 kHz is 100 km, which is comparable to the ionospheric height. As described in Subsection 4.3 the distance to the source is of the order of a few hundred kilometers, so that the incident wave at the bottom of the ionosphere even at 1 kHz can be considered as a far field. Furthermore, the ratio of the antenna length to the wavelength is increasing with frequency. The antenna radiation efficiency is improved with increasing its frequency when the length is shorter than one quarter wavelength. Therefore, we can show that the higher harmonic field at the VLF band may be significantly radiated from the same harmonic source of 24.4 Hz.

Park and Chang (1978) showed that the magnetospheric emissions can be stimulated even by a small total radiation power of 0.5 W using the Siple transmitter. They also estimated the input power into the

50-km diameter duct as 6×10^{-12} W/m^2 at the ionospheric height. Based on our observation result, in Fig. 5, the amplitudes of higher harmonics more than 10th order are approximately 5×10^{-7} A/m. Higher harmonics more than 1 kHz seems existing at the same amplitude because of the flat spectrum. The harmonic field at a few kHz can be estimated as $E = 1 \times 10^{-4}$ v/m and $H = 5 \times 10^{-7}$ A/m (0.6 pT), provided that the actual electric field strength can be estimated from the magnetic field strength. Therefore, the estimated flux at the bottom of the ionosphere is 1×10^{-10} W/m^2. Taking the same area of 2×10^9 m^2 and transmission coefficient of 5% as those used by Park and Chang (1978), the total input power into the duct is calculated as 0.01 W. This value is comparable to 0.0125 W that is estimated by Park and Chang (1978). Therefore, the triggering effect in the magnetosphere may be anticipated.

4.5 Initial result in comparison with satellite survey data over the Kola region

It has been demonstrated by Bullough *et al.* (1976), Luette *et al.* (1977), Yoshino *et al.* (1989) and Parrot (1990), using the satellites ARIEL 3 and 4, OGO 3, OHZORA, and AUREOL-3, respectively, that

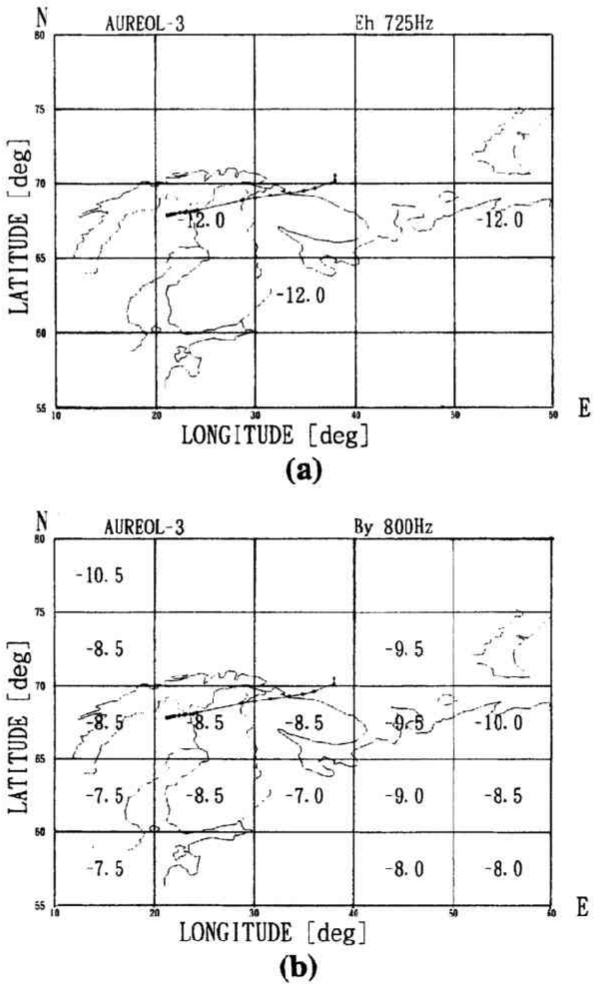

Fig. 13. (a) Average electric field (E_h) intensity in dB at 725 Hz observed by AUREOL-3, which is extracted from Fig. 6 of Parrot (1990). (b) Average magnetic field (B_y) intensity in dB at 800 Hz observed by AUREOL-3, which is extracted from Fig. 7 of Parrot (1990). Note that the empty box indicates less intensity than threshold of −13 and −11 for E_h and B_y, respectively.

the enhancement of the electromagnetic fields at ELF/VLF frequencies are caused by PLHR. Although the close relation between PLHR and magnetospheric emissions is indicated in a global scale, one-to-one correlation between the satellite observation and the ground source has not been clearly shown because power lines are usually made up by large distributed networks and they cannot be divided into independent segments.

Fortunately, as the observation period of AUREOL-3 covered the entire year of 1982 and its space resolution of approximately 500 km is enough to analyze the correlation (Parrot, 1990), we have looked to the distribution maps whether any enhancement on the map of the satellite observation can be related to our results. To show correlations with the local distribution around the Kola Peninsula, we have extracted the small parts from Figs. 6 and 7 of Parrot (1990). Figure 13(a) shows the electric field (E_h) intensity at 725 Hz, and Fig. 13(b) the magnetic field (B_y) intensity at 800 Hz. The intensity is indicated in dB in each box. The empty box indicates that the average intensity is less than threshold of −13 and −11 dB for E_h and B_y, respectively. (See Parrot (1990) in details.) Relative enhancements around the Kola Peninsula can be identified both in Figs. 13(a) and 13(b). The Kola Peninsula is contained within the range of highly sensitive magnetic latitudes where Luette *et al.* (1977) pointed out that ELF emissions were affected by PLHR. If harmonic radiations were transmitted into the magnetosphere, there would be triggered emissions like chorus. As the higher harmonic frequencies around 800 Hz is radiated from the new-type source, the enhancement in the Parrot's map around Murmansk can be interpreted as the result of direct propagation or of triggered emissions of the harmonic source of 24.4 Hz in the magnetosphere. If we can discriminate a starting frequency or a localized enhancement over the Kola region from other emissions excited by normal PLHR sources, some features of the PLHR-triggering process by the new-type source can be easily identified by its spectral characteristic. Lateral shifts with respect to the maximum point on the balloon, i.e. around Murmansk city, can be interpreted by a propagation effect of triggered emissions in the magnetosphere or by a sampling effect of the AUREOL-3 satellite. Detailed comparisons with the distribution map and the spectra are now in progress.

5. Conclusion

A new-type PLHR source characterized by (a) the fundamental frequency, (b) the harmonic spectrum, and (c) the isolation from the commercial power lines, is described in this paper. The characteristic electromagnetic field was observed over the Kola Peninsula during the flight of the balloon B_{15}-2N in 1982. The magnetic fields at the characteristic fundamental frequency of 24.4 Hz and its harmonic frequencies were clearly observed and its corresponding electric field was not detected above the internal noise level. The magnetic field showed a gradual increase, a broad single peak, and a relatively steep decrease along the flight trajectory.

Spectral lines at all harmonic frequencies of 24.4 Hz were observed continuously up to 1 kHz, furthermore, the integrated waveform of the observed magnetic field was consisted of the sinusoidal and impulsive waves. Based on the spectral characteristics, it is concluded that two possible sources, 1) single-phase transmission line and 2) electric railroad, are suggested as a generation mechanism. The frequency of 25 Hz has been used in the electric railroad. Additionally the frequency difference between 24.4 and 25 Hz can be explained by the difference at an isolated power generator. On the other hand, the source can be explained by the model calculation as a horizontal magnetic dipole (HMD) or a horizontal electric dipole (HED), based on the observed low impedance field. The two source models are consistent with the two possible mechanisms, i.e. a single-phase transmission line and an electric railroad. Comparing the estimated upper limit of the wave impedance of 30 Ω with the results of the model calculation, it is shown that the source distance should be approximately 100 to 150 km from the balloon trajectory. Therefore, it can be concluded that an electric railroad system driven by an isolated power generator is the most probable source placed on the Kola Peninsula.

The radiation power of this new-type source into the magnetosphere at a few kHz is estimated by using the observed spectral characteristics and the source distance. The estimated radiation power into the

magnetosphere seems comparable to that of Park and Chang (1978) for the PLHR simulation experiment performed at the SIPLE station in Antarctica. Based on the observation results of the AUREOL-3 satellite (Parrot, 1990), the enhancement of electromagnetic field at approximately 800 Hz can be roughly identified around the Kola Peninsula. Hence, it is concluded that the harmonic field of 24.4 Hz might be a potential source of magnetospheric emissions triggered by PLHR. It is important to note that the new-type source has a quite different spectral characteristics from the normal PLHR source of the commercial power lines because the fundamental frequency is half the commercial power line frequency and because the harmonic spectral lines seem continuously existing up to the VLF range. Further studies to investigate a correlating enhancement in satellite observations, and detailed estimations of the source location and its electrical parameter are necessary to understand the connection between the new-type source and magnetospheric emissions in the Kola region.

Other possibility of an artificial source used for deep electromagnetic sounding of the geological structure with a high power MHD generator (Heikka *et al.*, 1984) is investigated, however, its spectral characteristic is somewhat different from our observation and it was not operated at that time (Zhamaletdinov, private communication, 1994). However, such an experimental source can be a possible radiator in the ELF/VLF band. It is, of course, necessary further investigations on the actual source characteristics such as the location and the physical mechanism by detailed model calculations as well as by literatures. If the physical parameters can be determined precisely and the magnetospheric triggered emissions can be identified, it is useful to interpret the wave particle interaction process in the magnetosphere.

We would like to thank Drs. H. Yamagishi, T. Ono, H. Miyaoka and M. Ejiri of the National Institute of Polar Research (NIPR), Japan, and Dr. H. Fukunishi of Tohoku University, who conducted the balloon investigation and the launching operation at Esrange, Sweden. We thank Dr. M. Parrot, Centre National de la Recherche Scientifique (CNRS), France, for his helpful discussion, and Dr. A. A. Zhamaletdinov, Institute of Geology, Academy of Science of Russia, for his helpful information. This observation was fully supported by the grant of NIPR.

REFERENCES

Bannister, P. R., Simplified formulas for ELF propagation at shorter distances, *Radio Sci.*, **21**, 529–537, 1986.

Bullough, K., Satellite observations of power line harmonic radiation, *Space Sci. Rev.*, **35**, 175–183, 1983.

Bullough, K., A. R. L. Tatnall, and M. Denby, Man-made e.l.f./v.l.f. emissions and the radiation belts, *Nature*, **260**, 401–403, 1976.

Denki-gakkai-tsuushin-kyou-iku-kai, *Denki-Tetsu-Do*, pp. 4–7, Denki-Gakkai, Tokyo, 1976 (in Japanese).

Fukunishi, H. and H. Miyaoka, *Summary Report on International Balloon Campaign in Sweden and Norway, 1980–1982*, National Institute of Polar Research, Japan, March, 1984.

Galejs, J., *Terrestrial Propagation of Long Electromagnetic Waves*, pp. 74–149, Pergamon Press, Oxford, 1972.

Ginzberg, L. H., Extremely low frequency (ELF) propagation measurements along a 4900-km path, *IEEE Trans. Commun.*, **COM-22**, 452–457, 1974.

Heikka, J., A. A. Zhamaletdinov, S. E. Hjelt, T. A. Demidova, and Ye. P. Velikov, Preliminary results of MHD test registrations in northern Finland, *J. Geophys.*, **55**, 199–202, 1984.

Helliwell, R. A., J. P. Katsufrakis, T. F. Bell, and R. Ranghurum, VLF line radiation in the earth's magnetosphere and its association with power line radiation, *J. Geophys. Res.*, **80**, 4249–4258, 1975.

Katan, J. R. and P. R. Bannister, Summary of ELF propagation variations at mid and high latitudes during the November/December 1982 and February 1984 solar proton events, *Radio Sci.*, **22**, 111–124, 1987.

Luette, J. P., C. G. Park, and R. A. Helliwell, Longitudinal variations of very-low-frequency chorus activity in the magnetosphere: Evidence of excitation by power transmission lines, *Geophys. Res. Lett.*, **4**, 275–278, 1977.

Molchanov, O. A., M. Parrot, M. M. Mogilevsky, and F. Lefeuvre, A theory of PLHR emissions to explain the weekly variation of ELF data observed by a low-altitude satellite, *Ann. Geophys.*, **9**, 669–680, 1991.

Park, C. G. and D. C. D. Chang, Transmitter simulation of power line radiation effects in the magnetosphere, *Geophys. Res. Lett.*, **5**, 861–864, 1978.

Park, C. G. and R. A. Helliwell, Magnetospheric effect of power line radiation, *Science*, **200**, 727–730, 1978.

Parrot, M., World map of ELF/VLF emissions as observed by a low-orbiting satellite, *Ann. Geophys.*, **8**, 135–146, 1990.

Parrot, M., O. A. Molchanov, M. M. Mogilevski, and F. Lefeuvre, Daily variations of ELF data observed by a low-altitude satellite, *Geophys. Res. Lett.*, **18**, 1039–1042, 1991.

Tomizawa, I. and T. Yoshino, Distribution of horizontal magnetic field induced and radiated from power lines, *Bull. Inst. Space*

Aeronaut. Sci., Univ. Tokyo, **16**, no. 2(B), 1123–1132, 1980 (in Japanese).

Tomizawa, I. and T. Yoshino, Power line radiation over northern Europe observed on the balloon B_{15}-1N, *Mem. Natl. Inst. Polar Res.*, Spec. Iss. **31**, 115–123, 1984.

Tomizawa, I., T. Yoshino, and H. Sasaki, Geomagnetic effect on electromagnetic field strength of power line radiation over northern Europe observed on the balloons B_{15}-1N and B_{15}-2N, *Mem. Natl. Inst. Polar Res.*, Spec. Iss. **36**, 181–190, 1985.

Tomizawa, I., H. Sasaki, and T. Yoshino, Estimation on source characteristics of 24.4 Hz and its harmonics observed over the Kola Peninsula, Tech. Rep. IECJ, EMCJ87-85, 1987 (in Japanese).

Wait, J. R., *Electromagnetic Waves in Stratified Media*, 2nd ed., Pergamon Press, Oxford, 1970.

Yoshino, T. and I. Tomizawa, Rocket and balloon observations of power line radiation over Japanese Islands, in *Proc. 4th EMC Meeting, Zurich*, pp. 525–530, 1981.

Yoshino, T., I. Tomizawa, and K. Asami, Global distribution of power line harmonics radiation and natural VLF emission observed by the OHZORA satellite, in *Proc. of 8th EMC Symp., Zurich, 3–5 March, 1989*, pp. 7–12, 1989.